Excitation function measurements for the $^{12}C(^{20}Ne,^{12}C[0_2^+])^{20}Ne$ reaction

S. J. Hoad, N. M. Clarke, M. Freer, and B. R. Fulton
School of Physics and Astronomy, University of Birmingham, Edgbaston, Birmingham B15 2TT, United Kingdom

P. Fry and W. D. M. Rae
Department of Nuclear Physics, University of Oxford, Nuclear Physics Laboratory, Keble Road, Oxford OX1 3RH, United Kingdom

A. H. Wuosmaa
Physics Division, Argonne National Laboratory, Argonne, Illinois 60439
(Received 14 September 1998)

An excitation function for the $^{12}C(^{20}Ne,^{12}C[0_2^+])^{20}Ne$ reaction was measured over the energy range $E_{c.m.}=22.5-31.9$ MeV. An enhancement in the cross section was observed between $E_{c.m.}=24.5$ and 26.5 MeV in both the $^{12}C(0_2^+)+^{20}Ne(g.s.)$ and $^{12}C(0_2^+)+^{20}Ne(2^+)$ exit channels. Oscillatory angular distributions were observed at $E_{c.m.}=25.24$, 26.56, 28.50, and 30.44 MeV and the range of dominant angular momenta involved at these energies was found to be centered on $14\hbar, 15\hbar, 16\hbar$, and $17\hbar$, respectively. Excitation functions were also measured for the $^{12}C(^{20}Ne,^{12}C[3^-])^{20}Ne^*$ reaction. For the $^{12}C(^{20}Ne,^{12}C[0_2^+])^{20}Ne$ reaction the data were well described by the results of coupled channel calculations. [S0556-2813(99)07702-X]

PACS number(s): 25.70.Ef, 21.60.Gx, 27.30.+t, 27.20.+n

I. INTRODUCTION

Clustering in light alpha-conjugate nuclei has seen renewed interest in recent years, in particular with the possibility of highly deformed structures appearing at large excitation energies. The most deformed type of cluster structure predicted to exist are linear chain states constructed from alpha particles. These structures have been predicted by, for example, the alpha-cluster model (ACM) calculations of Marsh and Rae [1] and Nilsson-Strutinsky potential energy calculations of Leander and Larsson [2]. In the latter case such structures are stabilized by a microscopic shell-correction energy term, creating a pocket in the potential energy of the system.

There is also some experimental evidence for the existence of such highly deformed states in the lighter alpha-conjugate nuclei. The ground state of ^{8}Be has long been considered to be a linear chain of two alpha particles [3]. For ^{12}C the 0_2^+ state at $E_x=7.65$ MeV has historically been linked with a linear chain of three alpha particles [3,4], though the structure has also been suggested to be that of a slightly bent chain or extended isosceles triangle [5–8]. For ^{16}O an excitation function for the $^{12}C(\alpha,^8Be)^8Be$ reaction measured by Chevallier *et al.* [9] revealed several narrow resonances over the range of excitation energies $E_x(^{16}O)=17-21$ MeV, which had large partial widths for the decay of ^{16}O into ^{8}Be+^{8}Be. From the spins that were assigned to these resonances, it was suggested that they were members of a rotational band that possessed a large moment of inertia, consistent with a configuration comprising a linear chain of four alpha particles. Ames [10] observed similar resonances in $\alpha+^{12}$C scattering measurements, where the ^{12}C was excited to the 0_2^+ state. As this state in ^{12}C is considered to possess an extended alpha cluster structure, these resonances may be the nonsymmetric decay of the four-alpha chain in ^{16}O. More recently, a measurement of the $^{12}C(^{16}O,4\alpha)^{12}C$ reaction was performed by Freer *et al.* [11]. Some of the resonances that were observed in the breakup of $^{16}O^*$ into four α particles also could be linked with the decay of a deformed ^{16}O configuration.

Interestingly, an investigation of the inelastic scattering reaction $^{12}C(^{12}C,^{12}C[0_2^+])^{12}C[0_2^+]$ by Wuosmaa *et al.* [12] revealed a single broad peak in the measured excitation function. This peak was $\sim$4.7 MeV wide and centered at $E_x=46.4$ MeV, close to the predicted energy of the ''6-α'' chain state in ^{24}Mg [1]. Resonance phenomena are typically observed in reactions in which the entrance and exit channel grazing angular momenta are well matched; for the above reaction the mismatch is $6\hbar$. It has been suggested that this mismatch is overcome since the final state nuclei are produced in the highly deformed 0^+, 7.65 MeV state [12], further indicating a connection of the resonance with an extended configuration. Alternative explanations of this behavior in terms of direct reaction processes have also been suggested [13–15]. A subsequent search for a 7α chain state has also failed to provide evidence for such a state in ^{28}Si around the energy region predicted by the ACM calculations [16].

Although definitive conclusions are difficult concerning the existence of these chain states without the observation of the γ-ray emission from the intraband transitions, it does appear that the $^{16}O,4\alpha$ chain may represent the limit to which it is possible to find these extreme structures. The stability of such a structure relies upon a significant shell-correction energy to create a pocket in the nuclear potential, and this correction diminishes with increasing deformation. However, less extreme but still highly deformed structures may survive. For example, ACM calculations by Zhang, Merchant, and Rae [17] predict a highly deformed α-cluster structure in ^{32}S at an excitation energy $E_x\sim45.5$ MeV with a rotational gradient of $\hbar^2/2\mathfrak{I}=34$ keV/$\hbar^2$. These authors suggest that this structure is based on a $^{20}Ne(g.s.)+3\alpha$ configu-

TABLE I. Distances of detectors from target and the central angles of detectors.

Detector	Distance from target (mm)	Center of detector (degrees)
1	202	15.0
2	179	35.1
3	149	56.3
4	201	21.3
5	179	41.4
6	151	65.1

ration, with an overlap with ^{20}Ne+^{12}C(0_2^+), where the prolate deformation axis of the deformed ^{20}Ne nucleus is aligned with that of the ^{12}C chain structure. Leander and Larsson [2] also find a minimum in their Nilsson-Strutinsky calculations for ^{32}S that would correspond to this structure.

A previous measurement of the elastic and inelastic (^{12}C[2^+],^{20}Ne[2^+ and 4^+]) scattering of ^{20}Ne from ^{12}C, by Shapira *et al.* [18], revealed a small broad resonance ($\Gamma \sim 1$ MeV) at $E_{\text{c.m.}} \sim 27.8$ MeV [$E_x(^{32}\text{S}) = 46.7$ MeV]. This resonance is close to the energy at which ACM calculations predict this highly deformed state to exist. If this is the case, then the resonance should be enhanced in the ^{20}Ne $+ ^{12}$C(0_2^+) exit channel. This paper describes a measurement of the ^{12}C(^{20}Ne,^{12}C[0_2^+])^{20}Ne reaction cross section over the relevant energy range.

II. EXPERIMENTAL DETAILS

The experiment was performed using the ATLAS facility at the Argonne National Laboratory. A 4–8 pnA ^{20}Ne beam was used to bombard a 37 μg/cm^2 carbon foil. An excitation function was measured over the energy range $E_{\text{c.m.}} = 22.5$–31.9 MeV, with steps of approximately $\Delta E_{\text{c.m.}} = 0.5$ MeV. The ^{12}C(0_2^+) state is unbound to decay with respect to ^{8}Be+α; so the measurement of the ^{20}Ne+^{12}C(0_2^+) channel involves the detection of all three α particles from the ^{12}C decay. An array of six double-sided silicon strip detectors (DSSSD's), each 2500 mm^2 in area and 500 μm thick, was used for the experiment, with three detectors placed on either side of the beam. All detector faces possessed 16 strips each 3 mm wide with the direction of the strips on the front and back faces mutually perpendicular. Such detectors are ideal for breakup reactions, as the detection of multiparticle events within a single detector as well as between different detectors is possible [19]. The detectors had front and back face energy thresholds of 3.7 MeV and 2.4 MeV, respectively, and energy resolutions of 200 keV. The resolution with which it was possible to associate events in strips on both detector faces, and thus infer the emission angle for multiple hits, was thus $\sim$250 keV. The angular resolution was limited by the angle subtended by one 3 mm square ''pixel,'' which was typically $\Delta\theta_{\text{lab}} \sim 1°$. Table I lists the distances of the detectors from the target and their angles. The strip detectors were positioned so as to cover the center-of-mass range $18° \leqslant \theta_{\text{c.m.}} < 155°$ for the ^{12}C(^{20}Ne,^{12}C[0_2^+])^{20}Ne reaction. The energy calibration of the detectors was performed using sequential α decays of a ^{228}Th source and elastic scattering of ^{20}Ne from a ^{197}Au target. In addition, two small silicon detectors were placed at $\theta_{\text{lab}} = 8.8°$ to measure the elastic scattering yields and the beam energy. A Faraday cup was used to measure the integrated beam current.

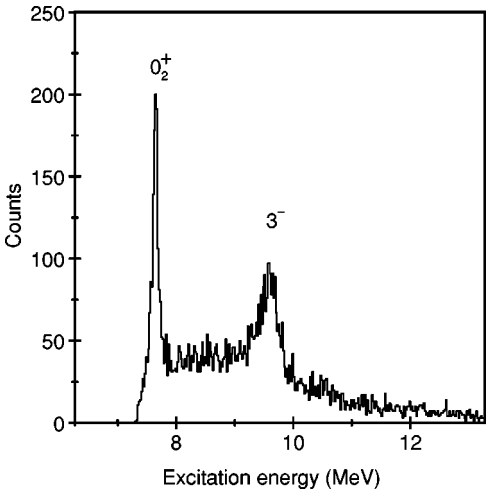

FIG. 1. Reconstructed excitation energy of the ^{12}C* nucleus from the 3α decay.

III. RESULTS.

For events in which there were a total of three hits in the three detectors on either side of the beam axis, the momentum of each particle was deduced from the recorded energy

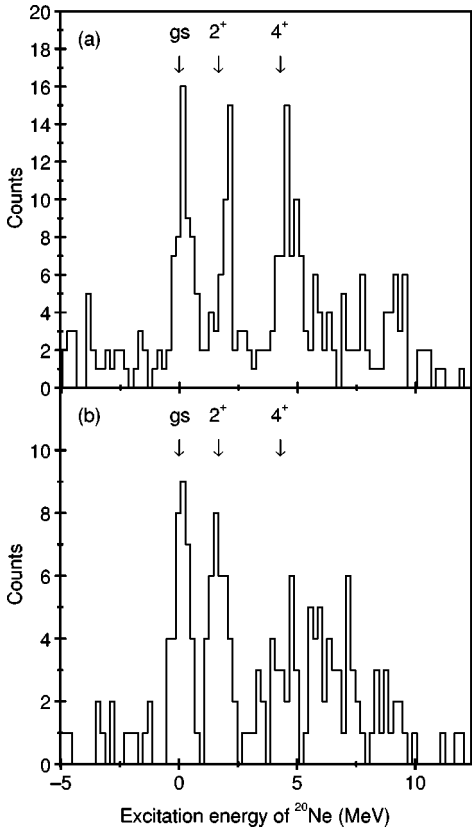

FIG. 2. Excitation energy spectrum for the undetected ^{20}Ne after gating on the (a) ^{12}C(0_2^+) state and (b) ^{12}C(3^-) state, $E_{\text{beam}} = 74.4$ MeV.

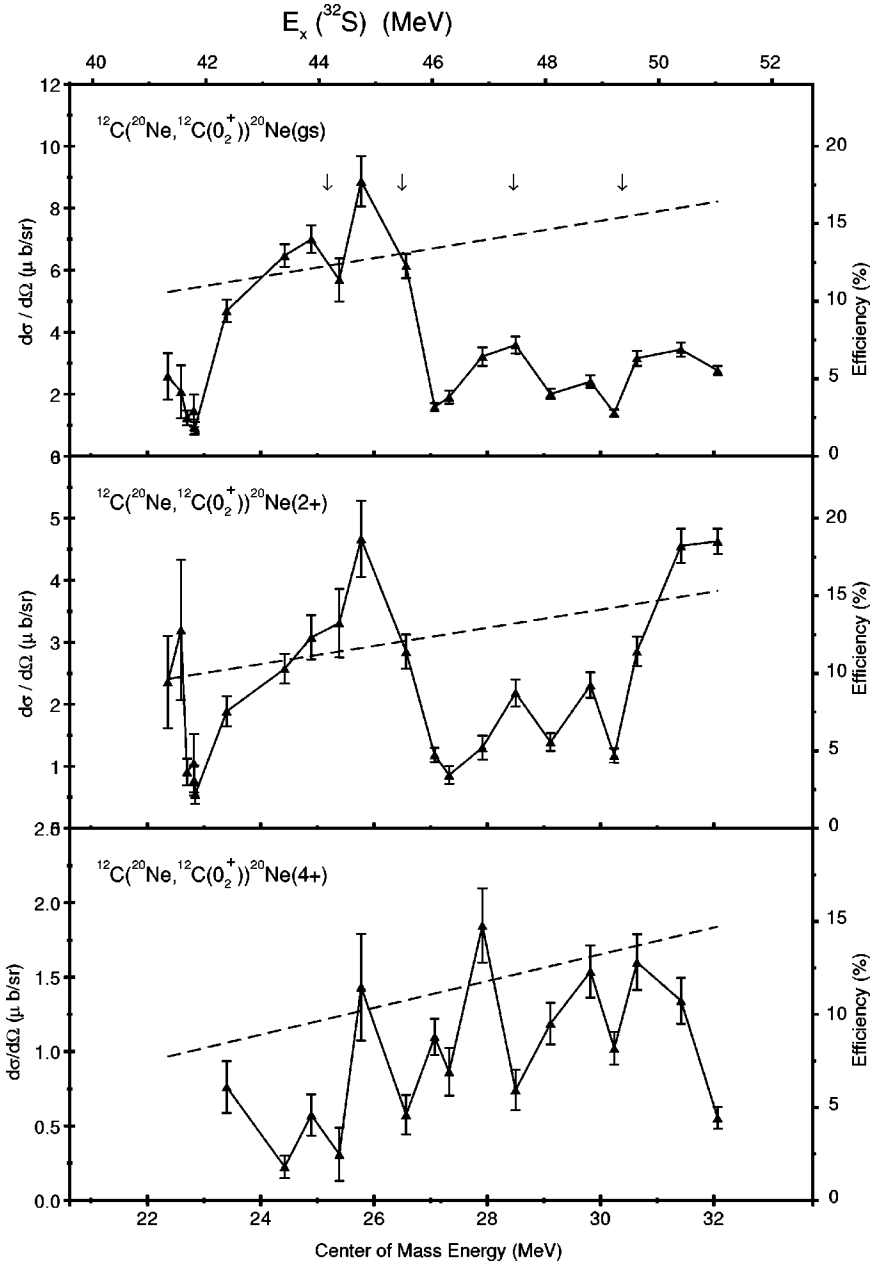

FIG. 3. Excitation function for the reaction $^{12}C(^{20}Ne,^{12}C[0_2^+])^{20}Ne^*$. The cross sections have been summed across the range $\theta_{c.m.} = 100° - 140°$. The dashed line is the calculated detection efficiency. The arrows indicate the energies where the angular distributions were determined.

and position, assuming that the three particles were ^{4}He nuclei produced from the decay of the ^{12}C nucleus. The excitation energy of the ^{12}C* nucleus was calculated using the relationship

$$E_x(^{12}\mathrm{C}^*) = 7.2 - \frac{P(^{12}\mathrm{C}^*)^2}{2\times 12.0} + \sum_{i=1}^{3} E_i(\alpha) \quad \text{(MeV)}, \quad (1)$$

where $P(^{12}C^*)$ was calculated from the momentum of the three alpha particles. A typical ^{12}C excitation energy spectrum is shown in Fig. 1. Two excited states can be identified, the 0_2^+, 7.65 MeV state [full width at half maximum (FWHM) = 0.2 MeV] and the 3^-, 9.63 MeV state (FWHM = 1 MeV). The difference in resolution is due to the larger opening angle of the three alpha particles emitted in the 3^- decay compared to that for the 0_2^+ state, which leads to an increased uncertainty in the reconstructed excitation energy. The background in this spectrum originates from events in which either one of the three alpha particles has been misidentified or from 3α coincidences which do not arise from the decay of ^{12}C.

Using software gates to select only one of the states observed in Fig. 1, and applying the principles of conservation of momentum and energy, the energy of the undetected recoiling ^{20}Ne nucleus was deduced, and hence the reaction Q value was determined:

$$E_{^{20}\mathrm{Ne}} = \frac{(\mathbf{P}_{\mathrm{beam}} - \mathbf{P}_{^{12}\mathrm{C}})^2}{2\times M_{\mathrm{Ne}}}, \quad (2)$$

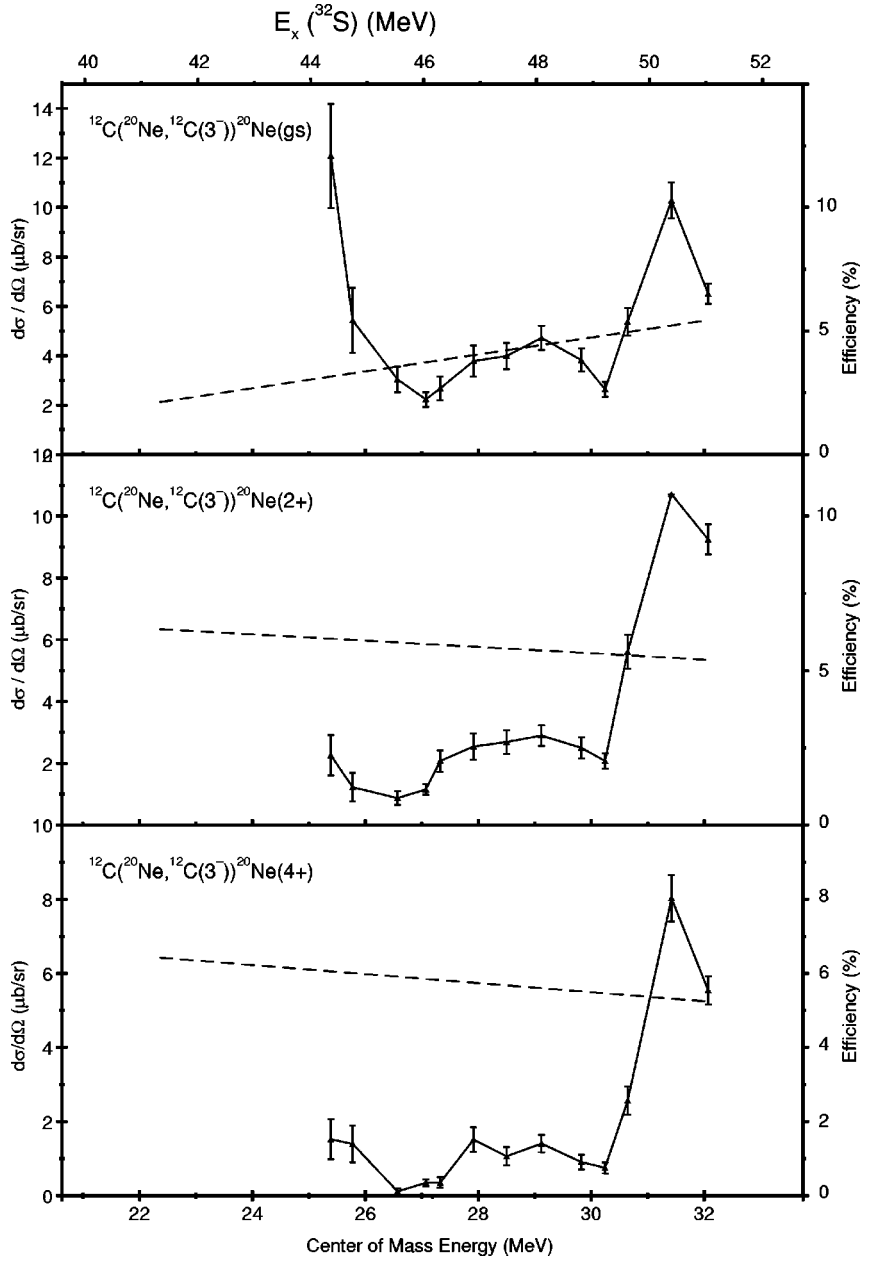

FIG. 4. Excitation function for the reaction $^{12}C(^{20}Ne,^{12}C[3^-])^{20}Ne^*$. The cross sections have been summed across the range $\theta_{c.m.}=100°-140°$. The dashed line is the calculated detection efficiency.

$$Q_{\text{value}}=E_{12_C}+E_{20_{Ne}}-E_{\text{beam}}. \tag{3}$$

A representative Q-value spectrum appears in Fig. 2. Three members of the ^{20}Ne ground state rotational band are observed, which are the 0^+ (0.00 MeV), 2^+ (1.63 MeV), and 4^+ (4.24 MeV) states.

For each of these three states, differential cross sections were calculated at each energy in order to construct excitation functions. The normalization of these data was performed using integrated beam current. The accuracy of the normalization was verified using the monitor detectors and $^{12}C+^{20}Ne$ elastic scattering yields, which also confirmed that the thickness of the target did not significantly change during the experiment. The cross sections, which are shown in Figs. 3 and 4, were corrected for the 3-α detection efficiency. The detection efficiencies were determined using a Monte Carlo calculation, which simulated the response of the detection system to the 3-α decay of the ^{12}C nucleus. The code determined the efficiency of detecting the three alpha particles from the decay of $^{12}C(0_2^+)$ using isotropic center-of-mass angular distributions for the $^{12}C\rightarrow{}^{8}Be+\alpha$ and $^{8}Be\rightarrow\alpha+\alpha$ reactions, and a $1/\sin\theta$ distribution (where θ is the emission angle in the ^{12}C center-of-mass system) was used to approximate the nonisotropic decay of the 3^- state. The resulting detection efficiency is shown as the dash curve in Figs. 3 and 4 for the reactions $^{12}C(^{20}Ne,^{12}C[0_2^+])^{20}Ne^*$ and $^{12}C(^{20}Ne,^{12}C[3^-])^{20}Ne^*$, respectively.

The excitation functions for the $^{12}C(0_2^+)+^{20}Ne$ channels show evidence for some structure, particularly in the ^{20}Ne(g.s.) and $^{20}Ne(2^+)$ yields. A significant enhancement in cross section is observed between $E_{c.m.}=24.5-26.5$ MeV (almost a factor of 5 higher than the yield at neighboring

energies) and this structure appears to be correlated between the $^{12}C(0_2^+)+^{20}Ne(g.s.)$ and $^{12}C(0_2^+)+^{20}Ne(2^+)$ channels. A small peak also appears at $E_{c.m.}\sim 28.5$ MeV which may be associated with a resonance that had been observed in the inelastic scattering measurements of Shapira *et al.* [18]. There is also some indication of an increase in the cross section, particularly in the $^{12}C(0_2^+)+^{20}Ne(2^+)$ reaction, between $E_{c.m.}=30$ and 32 MeV. For $E_{c.m.}<25$ MeV the 3^- state could not be clearly identified. The measured $^{12}C(3^-)+^{20}Ne$ excitation functions do not exhibit the same structure that was observed in the 0_2^+ channels. It should be noted, however, that the yield is rising in the $3^-+^{20}Ne$ reactions at approximately the same energy as that for the $^{12}C(0_2^+)$ excitation. There is possible evidence for a broad peak centered at $E_{c.m.}\sim 28$ MeV as observed in the 0_2^+ channels; however, this is wider than the one observed in the $^{12}C(0_2^+)+^{20}Ne(g.s.)$ and $^{12}C(0_2^+)+^{20}Ne(2^+)$ excitation functions and is thus likely to be unrelated.

In the $^{12}C(^{20}Ne,^{12}C[0_2^+])^{20}Ne(g.s.)$ reaction, all of the particles in the entrance and exit channels have zero spin; so the angular distributions of the reaction products are characterized by the angular momentum of the ^{32}S center-of-mass system and may be used to indicate resonant behavior. The angular distributions for the $^{12}C(0_2^+)+^{20}Ne(g.s.)$ channel are shown in Fig. 5. These cross sections have been corrected for the detection efficiency evaluated using the Monte Carlo simulation of the reaction and detection processes, where the efficiency was calculated as a function of the $^{12}C(0_2^+)$ center-of-mass emission angle. The errors shown are statistical; the magnitude of the systematic uncertainty of the Monte Carlo calculation is estimated to be 30%. Periodic oscillatory structure, indicative of a single dominant partial wave, was observed at four particular energies, $E_{c.m.}=25.2$, 26.5, 28.8, and 30.4 MeV. At other energies the angular distributions exhibited irregular structure, suggesting contributions from many angular momenta. Interestingly, these four energies also correspond to the appearance of structures in the excitation function and thus would be candidates for resonances. However, it is noteworthy that although the detectors span the center-of-mass angular interval 18°–155°, the data are limited to only 80°–155° despite the detection efficiency being largest over the region of smaller center-of-mass scattering angles. This indicates that the magnitude of the reaction yield is decreasing with increasing ^{20}Ne scattering angle. Although the angular distributions show oscillatory structure possibly characteristic of a squared Legendre polynomial, the cross section falls off more rapidly than $1/\sin\theta$, indicating that several partial waves are contributing. Thus the oscillatory behavior is diffractive in origin and does not indicate the presence of resonances. The limited angular coverage of the data does not enable us to uniquely assign a grazing partial wave, the competing possibilities differing by three units. The data indicate dominant partial waves centered on the following sequence of angular momenta: $E_{c.m.}=25.2$ MeV ($l=14/17\hbar$), 26.5 MeV ($15/18\hbar$), 28.8 MeV ($16/19\hbar$), and 30.4 MeV ($17/20\hbar$).

IV. DISCUSSION

The present data for the $^{12}C(0_2^+)+^{20}Ne(g.s.)$ final state have been compared with the results of previous measurements. Table II lists the center-of-mass energies and deduced angular momenta of these structures observed in the various reactions leading to a $^{12}C+^{20}Ne$ final state. The reactions included are $^{16}O(^{16}O,^{12}C)^{20}Ne$ [20,21], $^{16}O(^{16}O,^{12}C^*)^{20}Ne$ [22], and $^{12}C(^{20}Ne,^{12}C)^{20}Ne$ [23,18]. The corresponding excitation energy of the ^{32}S compound nucleus is also shown. The table indicates that a number of resonancelike structures have been observed in this region of excitation energy for ^{32}S. Apart from two of the angular momenta measured by Ford *et al.* [23], $l=14\hbar$ at $E_{c.m.}=27.9$ MeV and $l=15\hbar$ at $E_{c.m.}=27.2$ MeV, the other measurements appear to be largely consistent in terms of the sequence of energies and angular momenta. It is difficult to identify precisely structures in these data which can be related to those in the present measurements, and this is made more difficult as it is not possible to assign precise values of angular momenta to the present data. Figure 6 presents a comparison of measured energies and spins from Table II with the $^{20}Ne+^{12}C$ grazing

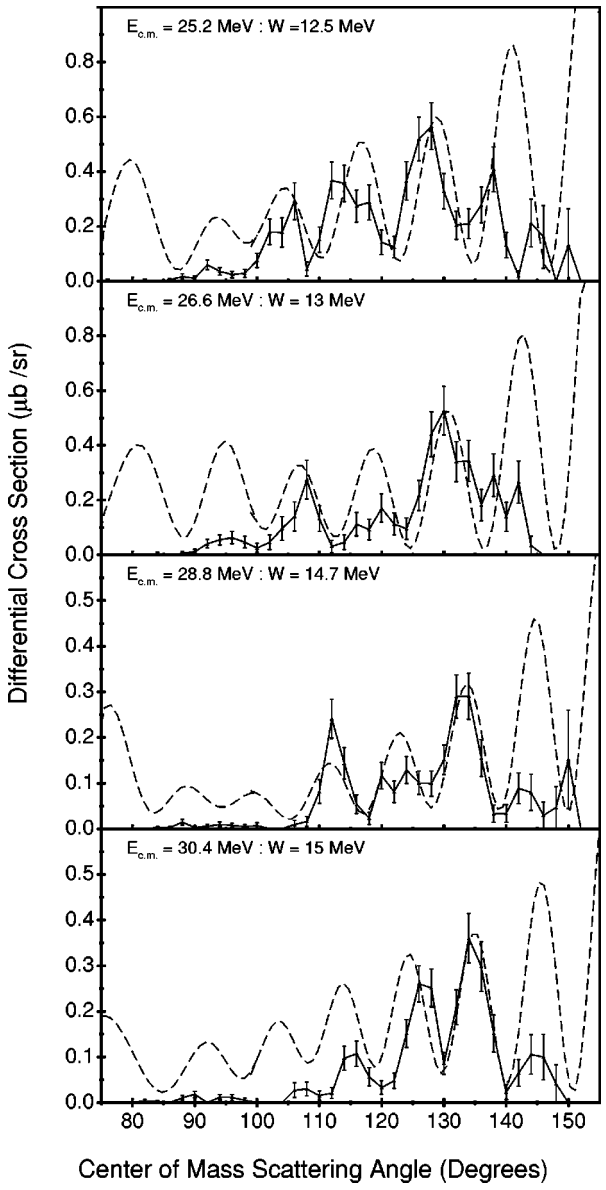

FIG. 5. Angular distributions overlaid with the calculated coupled channels cross sections. The value of the imaginary potential is indicated for each case.

TABLE II. Excitation energies and angular momenta from previous measurements compared with those from the present data.

Reaction	Ref.	$E_{c.m.}$/MeV	Ex(^{32}S)/MeV	l
^{16}O(^{16}O,^{12}C)^{20}Ne	[19]	23.0	39.5	16
		26.5	43.0	18
^{16}O(^{16}O,^{12}C)^{20}Ne	[20]	26	43	
		30	47	
^{16}O(^{16}O,^{12}C*)^{20}Ne	[21]	27.5	44.0	18
		32.0	48.5	20
^{12}C(^{20}Ne,^{12}C)^{20}Ne	[22]	21.38	40.34	
		23.63	42.59	
		27.23	46.19	15
		27.75	46.70	14
		28.20	47.16	19
^{12}C(^{20}Ne,^{12}C)^{20}Ne	[17]	27.75	46.72	
^{12}C(^{20}Ne,^{12}C[0_2^+])^{20}Ne	Present work	25.24	44.21	14/17
		26.56	45.53	15/18
		28.81	47.78	16/19
		30.44	49.41	17/20

angular momenta calculated using the optical model (solid line) [24]. The optical model parameters were adapted from Ref. [25], and are shown in Table III. For the present analysis, the imaginary potential was decreased from 23.9 to 15 MeV in order to account for the lower absorption as the center-of-mass energy was reduced from 146.3 MeV (as in Ref [25]) to ~30 MeV. There is good agreement between most of the previously observed excitation function peaks

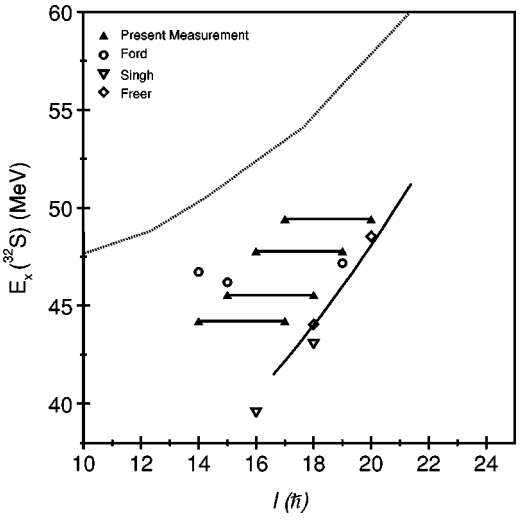

FIG. 6. Comparison of present data with that from previous measurements; see Table II. The symbols in the key indicate the different authors, and the curves are results of the theoretical calculations described in the text. The dotted line shows the result of ACM calculations [17] and the solid line shows the calculation of the grazing angular momentum using the modified Bohlen parameters [25] with W = 15 MeV.

TABLE III. Potential parameters used in coupled channel and optical model calculations.

Potential	V (MeV)	r_r (fm)	a_r (fm)	W (MeV)	r_i (fm)	a_i (fm)
Present work	175	0.775	0.924	15.0	1.107	0.85

and the grazing angular momentum trajectory. Furthermore, the present data also show a similar trend in increasing angular momentum with center-of-mass energy as the grazing angular momentum trajectory. This feature, in addition to the forward-peaked nature of the angular distributions, indicates that the reaction cross section is dominated by direct inelastic scattering. The dotted line in Fig. 6 shows the ACM calculations of the deformed ^{32}S structure corresponding to the aligned ^{12}C(0_2^+)+^{20}Ne configuration [17]. Clearly the rotational behavior of this structure is not reproduced by the present data.

In order to confirm the assumption that the data are dominated by direct inelastic scattering, coupled channel calculations were performed using the coupled channels reaction model code CHUCK97 [26]. In these calculations the ^{12}C and ^{20}Ne ground states were coupled to the 2^+ (4.43 MeV), 0_2^+ (7.65 MeV), and 3^- (9.63 MeV) states in ^{12}C and the 2^+ (1.63 MeV) state in ^{20}Ne; this coupling scheme is illustrated in Fig. 7. The optical potential parameters used in these calculations are those shown in Table III, with deformation lengths listed in Table IV from Ref. [25]. The strength of the imaginary potential was assumed to be energy dependent with scaling:

$$W \simeq 11.5 + (E_{c.m.} - 22.5) \times 0.43 \quad \text{(MeV)}. \tag{4}$$

The results of these calculations are compared to the experimental angular distributions in Fig. 5. The calculations reproduce many of the features of the measured distributions including the magnitude and phase over the interval 100°–140°. For angles larger than 140° the experimental measurements are affected by the changing detection efficiency profile which decreases rapidly in this region, 150°

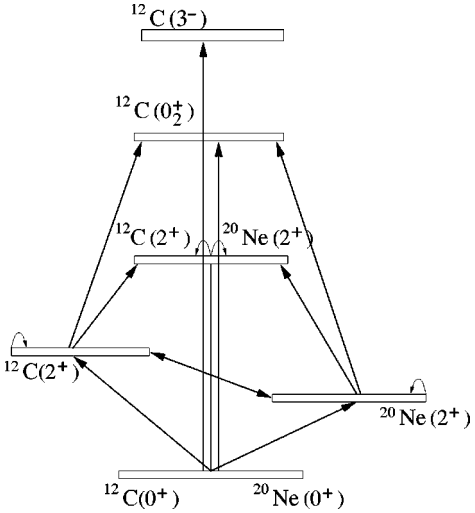

FIG. 7. The coupling scheme used in the coupled channel calculations.

TABLE IV. Deformation lengths used in the coupled channel calculations.

Coupling	Deformation length (fm)
g.s. $\leftrightarrow {}^{20}\mathrm{Ne}(2^+)$	
${}^{20}\mathrm{Ne}(2^+) \leftrightarrow {}^{20}\mathrm{Ne}(2^+)$	1.365
${}^{12}\mathrm{C}(2^+) \rightarrow {}^{20}\mathrm{Ne}(2^+)$	
g.s. $\leftrightarrow {}^{12}\mathrm{C}(2^+)$	
${}^{12}\mathrm{C}(2^+) \leftrightarrow {}^{12}\mathrm{C}(2^+)$	-1.465
${}^{20}\mathrm{Ne}(2^+) \rightarrow {}^{12}\mathrm{C}(2^+)$	
${}^{12}\mathrm{C}(2^+) \rightarrow {}^{12}\mathrm{C}(0_2^+)$	-0.279
${}^{20}\mathrm{Ne}(2^+) \rightarrow {}^{12}\mathrm{C}(0_2^+)$	

being the limit of observation. The reduced experimental cross section in this region is effected by the systematic uncertainties in the Monte Carlo calculation of the detection efficiency which are sensitive to the precise angular acceptance and energy thresholds of the detectors. There is also a departure of the calculated cross sections from the experimental yields below $\sim 100°$. We note that the present calculations are not fits to the experimental data, as owing to the absence of elastic and inelastic scattering data in this energy region there are no tuned scattering potentials which may be used to describe the ${}^{12}\mathrm{C}+{}^{20}\mathrm{Ne}$ interaction. Instead, we have used potentials and deformation lengths scaled from those developed for $E_{\mathrm{c.m.}}=146.3$ MeV. The magnitude of the cross sections in Fig. 5 at smaller ${}^{12}\mathrm{C}(0_2^+)$ center-of-mass emission angles (corresponding to larger center-of-mass emission angles for the ${}^{20}\mathrm{Ne}$ nucleus) is sensitive to the interference between one- and two-step processes and analysis of complete elastic and inelastic scattering measurements would be required to reproduce the data in this region.

The calculated partial wave decomposition of the scattering amplitudes shows that the dominant partial wave increases from $l_i=14\hbar$ to $17\hbar$ for $E_{\mathrm{c.m.}}=25$–30 MeV. The data for inelastic scattering to the ${}^{12}\mathrm{C}(0_2^+)+{}^{20}\mathrm{Ne}$ final state are consistent with partial waves two to three units smaller than the grazing partial wave.

Figure 8 shows the energy dependence of the coupled channel results for the ${}^{12}\mathrm{C}(0_2^+)+{}^{20}\mathrm{Ne}$ channel (dashed line) compared to the experimental data. The cross sections from the coupled channel calculations were summed over the range $100°$–$140°$, to coincide with the range of the measured angular distributions. The overall gross resonancelike structure at $E_{\mathrm{c.m.}}=24.5$–26.5 MeV is reproduced, in both magnitude and width. The ${}^{12}\mathrm{C}({}^{20}\mathrm{Ne},{}^{12}\mathrm{C}[0_2^+]){}^{20}\mathrm{Ne}$ inelastic scattering reaction is mismatched by three units of angular momentum and shows a particular sensitivity to other coupled reaction channels. Similarly, Hirabayashi *et al.* [13] were able to reproduce many of the features of the mismatched ${}^{12}\mathrm{C}({}^{12}\mathrm{C},{}^{12}\mathrm{C}[0_2^+]){}^{12}\mathrm{C}[0_2^+]$ reaction using the coupled channel approach.

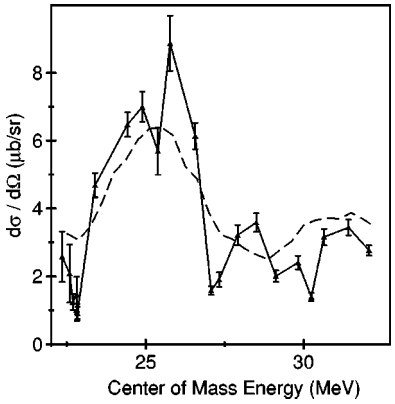

FIG. 8. The ${}^{12}\mathrm{C}({}^{20}\mathrm{Ne},{}^{12}\mathrm{C}[0_2^+]){}^{20}\mathrm{Ne}$(g.s.) reaction excitation function compared with the coupled channel calculations (dashed line). The experimental and theoretical cross sections have been summed across the range $\theta_{\mathrm{c.m.}}=100°$–$140°$.

V. CONCLUSIONS

The present excitation function measurement of the ${}^{12}\mathrm{C}({}^{20}\mathrm{Ne},{}^{12}\mathrm{C}[0_2^+]){}^{20}\mathrm{Ne}$ reaction over the center-of-mass energy interval $E_{\mathrm{c.m.}}=22.5$–31.9 MeV shows some evidence for broad structures. The angular distributions associated with these broad structures are oscillatory. The periodicity of these distributions at $E_{\mathrm{c.m.}}=25.24$, 26.56, 28.5, and 30.44 MeV can be characterized by a range of dominant angular momenta centered on $14\hbar$, $15\hbar$, $16\hbar$, and $17\hbar$, respectively. Many of the characteristics of the experimental data, including the energy and angular dependence, are well reproduced by coupled channel calculations of the inelastic scattering reaction ${}^{12}\mathrm{C}({}^{20}\mathrm{Ne},{}^{12}\mathrm{C}[0_2^+]){}^{20}\mathrm{Ne}$ without the inclusion of resonances. The present measurement thus finds no evidence for broad ($\Gamma>1$ MeV) features over the above energy region and consequently no evidence for a highly deformed ${}^{32}\mathrm{S},{}^{20}\mathrm{Ne}+3\alpha$ cluster structure.

ACKNOWLEDGMENTS

The authors would like to acknowledge the Engineering and Physical Sciences Research Council for financial support. The authors would also like to thank the ATLAS crew for providing the high quality ${}^{20}\mathrm{Ne}$ beams required for these measurements. The work of the Physics Division, Argonne National Laboratory is supported by the U.S. Department of Energy, Nuclear Physics Division, under Contract No. W-31-109-Eng-38.

[1] S. Marsh and W. D. M. Rae, Phys. Lett. B **180**, 185 (1986).
[2] G. Leander and S. E. Larsson, Nucl. Phys. **A239**, 93 (1975).
[3] D. M. Brink, in *Proceedings of the International School of Physics ''Enrico Fermi,''* Course XXXVI, Varenna, 1965, edited by C. Bloch (Academic, New York, 1966), p. 247.
[4] N. Takigawa and A. Arima, Nucl. Phys. **A168**, 593 (1971).
[5] H. Friedrich, L. Satpathy, and A. Weiguny, Phys. Lett. **36B**, 189 (1971).
[6] N. de Takascy, Nucl. Phys. **A178**, 469 (1972).
[7] Chr. Bargholtz, Nucl. Phys. **A243**, 449 (1975).

[8] D. V. Fedorov and A. S. Jensen, Phys. Lett. B **389**, 631 (1996).
[9] P. Chevallier, F. Scheibling, G. Goldring, I. Plesser, and M. W. Sachs, Phys. Rev. **160**, 827 (1967).
[10] L. L. Ames, Ph.D. thesis, University of Wisconsin, Madison, 1979, p. 250.
[11] M. Freer, N. M. Clarke, N. Curtis, B. R. Fulton, S. J. Hall, M. J. Leddy, J. S. Pople, G. Tungate, R. P. Ward, P. Simmons, W. D. M. Rae, S. P. G. Chappell, S. P. Fox, C. D. Jones, D. L. Watson, G. J. Gyapong, S. M. Singer, W. N. Catford, and P. H. Regan, Phys. Rev. C **51**, 1682 (1995).
[12] A. H. Wuosmaa, R. R. Betts, B. B. Back, M. Freer, B. G. Glagola, Th. Happ, D. J. Henderson, and P. Wilt, Phys. Rev. Lett. **68**, 1295 (1992).
[13] Y. Hirabayashi, Y. Sakuragi, and Y. Abe, Phys. Rev. Lett. **74**, 4141 (1995).
[14] S. P. G. Chappell *et al.*, Phys. Rev. C **51**, 695 (1995).
[15] R. A. Le Marechal, N. M. Clarke, M. Freer, B. R. Fulton, S. J. Hall, S. J. Hoad, G. R. Kelly, R. P. Ward, C. D. Jones, P. Lee, and D. L. Watson, Phys. Rev. C **55**, 1881 (1997).
[16] P. M. Simmons, W. D. M. Rae, S. P. C. Chappell, S. P. Fox, C. D. Jones, D. L. Watson, M. Freer, B. R. Fulton, N. M. Clarke, N. Curtis, M. J. Leddy, J. S. Pople, S. J. Hall, R. P. Ward, G. Tungate, W. N. Catford, G. J. Gyapong, S. M. Singer, and P. H. Regan, Phys. Rev. C **51**, 3500 (1995).
[17] J. Zhang, A. C. Merchant, and W. D. M. Rae, Nucl. Phys. **A575**, 61 (1994).
[18] D. Shapira, J. L. C. Ford, Jr., and J. Gomez del Campo, Phys. Rev. C **26**, 2470 (1982).
[19] A. H. Wuosmaa *et al.*, Nucl. Instrum. Methods Phys. Res. A **345**, 482 (1994).
[20] P. P. Singh, D. A. Sink, P. Schwandt, R. E. Malmin, and R. H. Siemssen, Phys. Rev. Lett. **28**, 1714 (1972).
[21] H. H. Rossner, G. Hinderer, A. Weidinger, and K. A. Eberhard, Nucl. Phys. **A218**, 606 (1974).
[22] M. Freer, N. M. Clarke, B. R. Fulton, S. J. Hoad, G. R. Kelly, R. A. Le Marechal, R. P. Ward, C. D. Jones, P. Lee, W. N. Catford, and G. J. Gyapong, J. Phys. G **22**, 1053 (1996).
[23] J. L. C. Ford, Jr., J. Gomez del Campo, D. Shapira, M. R. Clover, R. M. DeVries, B. R. Fulton, R. Ost, and C. F. Maguire, Phys. Lett. **89B**, 48 (1979).
[24] N. M. Clark, OPTIM94, optical model calculation program (unpublished).
[25] H. G. Bohlen, E. Stiliaris, B. Gebauer, W. von Oertzen, M. Wilpert, Th. Wilpert, A. Ostrowski, Dao T. Khoa, A. S. Demyanova, and A. A. Ogloblin, Z. Phys. A **346**, 189 (1993).
[26] N. M. Clarke, CHUCK97, coupled channels program (unpublished).